CrossMark

Persistence of SIV in the brain of SIV-infected Chinese rhesus macaques with or without antiretroviral therapy

Stefanie Perez[1,2] · Ann-Marie Johnson[1] · Shi-hua Xiang[3] · Jian Li[4] · Brian T. Foley[5] ·
Lara Doyle-Meyers[1] · Antonito Panganiban[1,6] · Amitinder Kaur[1,6] ·
Ronald S. Veazey[1,7] · Yuntao Wu[8] · Binhua Ling[1,6]

Abstract Persistence of HIV-1 reservoirs in the central nervous system (CNS) is an obstacle to cure strategies. However, little is known about residual viral distribution, viral replication levels, and genetic diversity in different brain regions of HIV-infected individuals on combination antiretroviral therapy (cART). Because myeloid cells particularly microglia are likely major reservoirs in the brain, and more microglia exist in white matter than gray matter in a human brain, we hypothesized the major viral reservoirs in the brain are the white matter reflected by higher levels of viral DNA. To address the issue, we used the Chinese rhesus macaque (ChRM) model of SIV infection, and treated 11 SIVmac251-infected animals including long-term nonprogressors with cART for up to 24 weeks. SIV reservoirs were assessed by SIV DNA levels in 16 specific regions of the brain and 4 regions of spinal cord. We found relatively high frequencies of SIV in basal ganglia and brain stem compared to other regions. cART-receiving animals had significantly lower SIV DNA levels in the gray matter than white matter. Moreover, a shortened envelope gp120 with 21 nucleotide deletions and guanine-to-adenine hypermutations were observed. These results demonstrate that SIV enters the CNS in SIV-infected ChRM with a major reservoir in the white matter after cART; the SIV/ChRM/cART is an appropriate model for studying HIV CNS reservoirs and testing new eradication strategies. Further, examining multiple regions of the CNS may be needed when assessing whether an agent is successful in reducing the size of SIV reservoirs in the CNS.

Keywords Human immunodeficiency virus · Simian immunodeficiency virus · Rhesus macaque · Central nervous system · Reservoir · Antiretroviral therapy

✉ Binhua Ling
  bling@tulane.edu

1   Tulane National Primate Research Center, 18703 Three Rivers Road, Covington, LA 70433, USA

2   Present address: Hayward Genetics Center, Tulane University School of Medicine, New Orleans, LA 70112, USA

3   Nebraska Center for Virology, School of Veterinary Medicine and Biomedical Sciences, University of Nebraska, Lincoln, NE 68583, USA

4   Department of Statistics, Tulane University School of Public Health and Tropic Medicine, New Orleans, LA 70112, USA

5   Theoretical Biology and Biophysics Group, Los Alamos National Laboratory, Los Alamos, NM 87545, USA

6   Department of Microbiology and Immunology, Tulane University School of Medicine, New Orleans, LA 70112, USA

7   Department of Pathology and Laboratory Medicine, Tulane University School of Medicine, New Orleans, LA 70112, USA

8   National Center for Biodefense and Infectious Diseases, Department of Molecular and Microbiology, George Mason University, Manassas, VA 20110, USA

Introduction

The central nervous system (CNS) is one of the major anatomic HIV reservoirs in many HIV-infected patients, even those on highly suppressive combination antiretroviral therapy (cART), making it a major obstacle to HIV eradication and a cure. HIV reaches the CNS as early as 8 days post-infection (Valcour et al. 2012). Although cART can effectively reduce HIV loads in cerebrospinal fluid (CSF), decreases are slower and delayed compared to viral loads in plasma. Further, despite low to absent levels in blood of patients on cART, residual viral RNA can often be detected in the brain, and serve as a persistent reservoir for viral replication, resulting in

neurocognitive dysfunction, despite the absence of direct neuronal infection (Heaton et al. 2010). Intensification of cART does not seem to have an impact on this low-level viral production in the CNS (Eden et al. 2010). Currently, no drugs are capable of eradicating HIV reservoirs from the CNS.

Many aspects of the HIV/SIV reservoirs in the CNS are still unclear (Brew et al. 2015; Churchill and Nath 2013). For instance, little is known regarding the cell types harboring persistent viruses, the distribution of virus and infected cells, viral diversity in tissues, or the possible genetic evolution in the brains of HIV-infected patients on cART. HIV diversity has been found in the brain of untreated patients showing neurological symptoms or opportunistic infections. Structural changes have also been observed in both the cerebral white and gray matters of HIV patients, even during suppressive cART in adults and adolescents (Fennema-Notestine et al. 2013). However, specifics of the distribution of HIV in white matter and gray matter are relatively unknown.

As different regions of the brain have different structure and function, the distribution and density of viral target cells is patchy, and the susceptibility of various regions of the brain to HIV infection differs. Few studies have extensively examined different regions of the CNS in HIV infection. A study of six brain tissues (meninges, frontal gray matter, frontal white matter, temporal subcortex, cerebellum, and basal ganglia) of HIV-infected patients demonstrated that all patients had HIV DNA in the brain, but with variable levels (Zhao et al. 2009). However, most studies have only examined one or two regions of the brain, which may not accurately reflect the whole extent of cerebral HIV infection. The challenge of studying multiple sections largely lies in the difficulties in accessing different, fresh brain tissues for sampling. To address these issues, animal models are essential.

Nonhuman primate (NHP) models have been instrumental in studying viral latency/persistence in the CNS (Clements et al. 2011) and continue to be used to address unanswered questions in the field (Garrido and Margolis 2015). In SIV-infected, treatment-naïve macaques, SIV DNA can be detected throughout SIV infection, but RNA is usually only detectable at the later stages of SIV encephalitis (Williams et al. 2001). In pigtailed macaques (*Macaca nemestrina*) infected with neurovirulent viruses SIV/17E-Fr or SIV/DeltaB670, cART reduces viral replication and inflammation, but viral DNA is persistently detectable (Zink et al. 2010). Further, viral compartmentalization occurs between the meninges and the brain parenchyma, and virus in CSF more closely matches that of virus in the meninges at least in one animal infected with neuropathogenic isolates SIVsmH631Br and SIVsmE804E (Matsuda et al. 2013). However, the density of SIV-infected cells can vary depending on the part of the brain sampled, which may confound interpretation of some studies, depending on what tissue sites and the number of sites

biopsied (Brew et al. 2015). Thus far, it remains unclear as to whether cART can alter the distribution and density of SIV infection and addressing these issues is critical for new strategies targeting specific tissues for viral control and eradication.

Chinese rhesus macaques (ChRM) have been used in SIV pathogenesis and therapy studies, but rarely has the CNS been studied in this model. Recently, one study detected SIVmac239 RNA in the brain of SIV-infected ChRM resulting in neuropathological damage (Liu et al. 2016). In this study, we used SIVmac251, the most commonly used virus in the NHP SIV/AIDS model, as it more closely mimics the pathogenesis of HIV infection. Because myeloid cells such as perivascular macrophages and microglia are likely major reservoirs in the brain (Churchill et al. 2016; Dahl et al. 2014; Schnell et al. 2009; Williams et al. 2001), and because more microglia exist in white matter than gray matter in the human brain (Mittelbronn et al. 2001), we hypothesized that the white matter may be a more significant viral reservoirs in the brain than the gray matter which should be evident by higher DNA levels in the former. To address these issues, we examined SIV viral load in different regions of the CNS, compared viral distribution and genetic diversity in both SIVmac251-infected ChRM without cART and in animals on cART at the end of therapy. We also analyzed SIV gp120 envelope viral sequences isolated from the CNS. To our knowledge, this is the first time that SIV CNS reservoirs have been carefully examined in 20 regions of the CNS in a ChRM model, which closely mimics HIV infection and treatment in humans (Ling et al. 2010; Ling et al. 2014; Ling et al. 2013; Ling et al. 2007; Ling et al. 2002a; Ling et al. 2002b; Zhou et al. 2013).

Results

Basic information of SIV-infected Chinese rhesus macaques with or without antiretroviral therapy

Eleven adult ChRM (four males and seven females) 7 to 22 years of age (mean age 13.9 ± 4.6 s.d.) were studied in the cART drug-treated (DTs) group. These animals were chronically SIVmac infected for 3–87.6 months prior to initiation of cART with relatively low plasma viral loads (pVL). Animals received three-drug antiretroviral therapy for varying periods of time ranging from 7 to 24 weeks. By the end of cART termination, all animals reached undetectable levels of pVL (limit of detection was 30 copies/ml) (Table 1). Another group of 12 animals (six males and six females) 6.6–14.5 years (mean age 10.2 ± 2.7 s.d.) was used for studies of plasma and CSF viral loads (cVL). These animals received cART for a short period of time (8 weeks) starting at 4 weeks post-SIV infection, but they were off of cART for varying

Table 1 Basic information of SIV-infected Chinese rhesus macaques on antiretroviral therapy

Animal ID	Age	Sex	Length of infection pre-ART (month)	Route of infection	pVL pre-ART (copies/ml)	Period of ART (weeks)	pVL at the end of ART (copies/ml)	pVL after off ART (copies/ml)	cVL at the end of ART
CM61	12.9	M	16.8	I.V.	3.73E + 04	24.0	UD	–	UD
DI98	11.7	M	16.8	I.V.	1.12E + 03	8.0	UD	–	UD
DT93	21.7	F	36.0	I.V.	3.28E + 03	10.0	UD	–	UD
EV57	16.6	F	3.0	I.V.	1.30E + 05	8.0	UD	–	UD
FA10	15.4	F	36.0	I.V.	1.90E + 02	24.0	UD	–	UD
FH20	8.8	M	16.8	I.V.	1.90E + 02	24.0	UD	–	UD
GD41	7.4	M	3.0	I.V.	3.90E + 05	8.0	UD	–	UD
GJ54	13.9	F	32.4	I.V.	1.54E + 03	8.0	UD	1.2E + 03[a]	UD
HG40	18.1	F	60.0	I.V.	2.87E + 04	11.0	UD	–	UD
IV30	8.6	F	31.2	I.V.	4.65E + 04	11.0	UD	–	UD
PO15	20.0	F	87.6	I.V.	3.46E + 02	7.0	UD	–	UD

Animals were on ART when euthanized

I.V. intravenously, *UD* undetectable, – unavailable, animals were on ART

[a] pVL rebound after 18 days of ART off

lengths of time when necropsied as shown in Table 2. All the viral loads on plasma and CSF shown were measured at the time of necropsy. No observable pathogenic lesions or evidence of SIV-associated encephalitis was detected by histologic examination.

CSF viral loads and their association with plasma viral loads in SIV-infected Chinese rhesus macaques CSF viral load (cVL) levels were tested in 12 untreated animals. The levels ranged from undetectable (limitation of detection, 30 copies/ml) to 5.6×10^5 copies/ml. Compared to plasma viral loads, CSF had much lower levels (median 802 copies/ml, 25–75% percentile range 30–63,275 copies/ml) than pVL (median 77,650 copies/ml, 25–75% percentile range 366–282,750 copies/ml). However, cVL in untreated animals

positively correlated with pVL levels ($R = 0.7686$, $p = 0.0049$) (Fig. 1). In the cART group, cVL were not detectable because these animals had pVL at $\sim 10^3$ copies/ml or less even prior to initiation of cART. In addition, although the ages of cART group were relatively older than that of the untreated group, analysis did not show significant correlation between age and pVL in each group; therefore, the impact of age discrepancy was considered insignificant in this study.

Frequency of positive SIV *env* DNA in different regions of the brain in animals with and without cART To determine distribution and frequency of SIV infection in different regions of the brain and spinal cord in both untreated animals and DTs, we collected 16 brain regions that included corpus callosum, temporal lobe, frontal lobe, parietal lobe, occipital

Table 2 Basic information of SIV-infected Chinese rhesus macaques

| Animal ID	Age	Sex	Length of infection (month)	Route of infection	Plasma VL (copies/ml)	CSF VL (copies/ml)
BV71	14.5	F	17.9	I.V.	2.7E + 02	3.0E + 04
CC57	12.8	M	16.8	I.V.	8.5E + 06	5.6E + 05
CK24	12.4	F	16.9	I.V.	2.2E + 05	1.4E + 03
DI62	12.3	M	17.0	I.V.	1.5E + 05	2.3E + 02
DP02	11.7	F	17.8	I.V.	3.8E + 02	UD
EM19	10.7	F	17.8	I.V.	1.3E + 03	2.8E + 01
EN60	10.3	M	17.2	I.V.	3.0E + 05	4.9E + 04
FJ69	9.3	M	16.6	I.V.	1.6E + 06	1.7E + 05
FR70	8.5	F	15.6	I.V.	3.6E + 02	UD
HC58	6.6	M	16.7	I.V.	UD	UD
HD94	6.6	M	16.7	I.V.	7.6E + 02	UD
IF29	6.9	F	30.3	I.V.	1.7E + 04	6.8E + 04

I.V. intravenously, *UD* undetectable
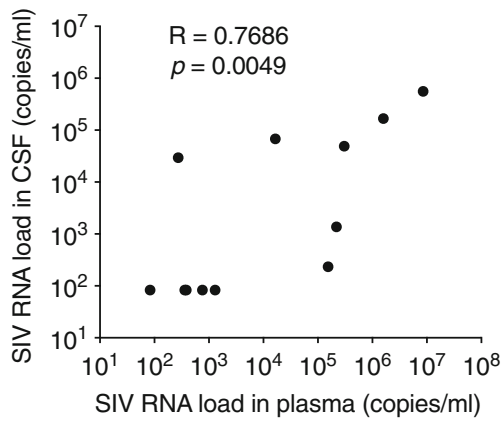
Fig. 1 Correlations between SIV RNA loads in plasma and cerebrospinal fluid (CSF) in untreated SIV-infected Chinese rhesus macaques

lobe etc., and four regions of the spinal cord (Table 3). We used nested PCR to amplify SIV envelope gp120 from the 16 brain regions and spinal cord in 11 cART animals and 2 typical progressors which had sustained pVL at 10^4–10^6 copies/ml off treatment (Table 3). Detectable viral DNA was spread throughout many brain regions from different individuals on cART, although 6 of 11 cART animals (55%) had no virus detected in the CNS. The highest frequency of detectable SIV DNA in cART group was in basal ganglia (4 of 11, 36.4%) followed by brain stem (3 of 11, 27.3%). Because the

regions of gray and white matter are not distinctly separated in midbrain, detection of SIV was not separated into gray and white matter in this region (Table 3). Not surprisingly, no SIV RNA was detected in any of the drug-treated animals.

SIV DNA levels were significantly reduced in gray matter but not in white matter in cART macaques compared to untreated animals To assess viral distribution in the gray and white matters, we used real-time PCR and quantified SIV *gag* DNA levels in the two untreated TPs and three DTs that showed SIV-positive signals in multiple regions of the brain. The detection limit of SIV *gag* DNA was 15 copies/10^6 cells. In DTs, virus DNA levels were significantly higher in white matter than in gray matter ($p < 0.0001$) (Fig. 2a). White matter had a median 455.7 copies/10^6 cells (25–75% percentile range 221–773 copies/10^6 cells), whereas gray matter had a median 50 copies/10^6 cells (25–75% percentile range 20–127.9 copies/10^6 cells). In contrast, gray matter had significantly higher viral levels than white matter in untreated SIV-infected animals ($p < 0.0001$) (Fig. 2b); the former with a median 4184 copies/10^6 cells (25–75% percentile range 1541–7697 copies/10^6 cells) and the latter with a median 472.5 copies/10^6 cells (25–75% percentile range 205.6–1190 copies/10^6 cells). Viral levels were significantly higher in the untreated group than treated group in gray matter ($p < 0.0001$) (Fig. 2c).

Table 3 Frequency of SIV *env* DNA detection in different regions of the CNS

Label	Brain region	Typical progressor (n = 2)		Animals on ART (n = 11)	
		Gray matter	White matter	Gray matter	White matter
19L	Corpus callosum—left	–	100%	–	9.1%
19R	Corpus callosum—right	–	100%	–	18.2%
20L	Temporal lobe—left	50%	100%	0.0%	18.2%
20R	Temporal lobe—right	100%	100%	0.0%	18.2%
21L	Frontal lobe—left	100%	100%	0.0%	9.1%
21R	Frontal lobe—right	100%	100%	9.1%	18.2%
22L	Parietal lobe—left	100%	100%	9.1%	18.2%
22R	Parietal lobe—right	100%	100%	0.0%	9.1%
23L	Occipital lobe—left	50%	100%	9.1%	18.2%
23R	Occipital lobe—right	100%	100%	18.2%	9.1%
24	Brain stem	100%		27.3%	
25	Basal ganglia	100%		36.4%	
26	Thalamus	100%		9.1%	
27	Hypothalamus	100%		18.2%	
28	Hippocampus	100%		18.2%	
29	Cerebellum	100%		0.0%	
	Spinal cord				
31	Cervical	50%		9.1%	
32	Thoracic	50%		0.0%	
33	Lumbar	50%		9.1%	
34	Sacral/coccygeal	50%		18.2%	

Fig. 2 Comparison of levels of SIV *gag* DNA between gray matter and white matter in the group of cART-treated (**a**) and untreated Chinese rhesus macaques (ChRM) (**b**), and levels of SIV *gag* DNA in gray matter between groups of untreated and cART-treated ChRM (**c**) and in white matter (**d**). Solid diamond, SIV *gag* DNA viral load in gray matter of ChRM on ART; solid square, SIV *gag* DNA viral load in white matter of ChRM on ART; open diamond, SIV gag DNA viral load in gray matter of untreated ChRM; open square, SIV *gag* DNA viral load in white matter of untreated ChRM; ***$p < 0.0001$, N. S. no significance
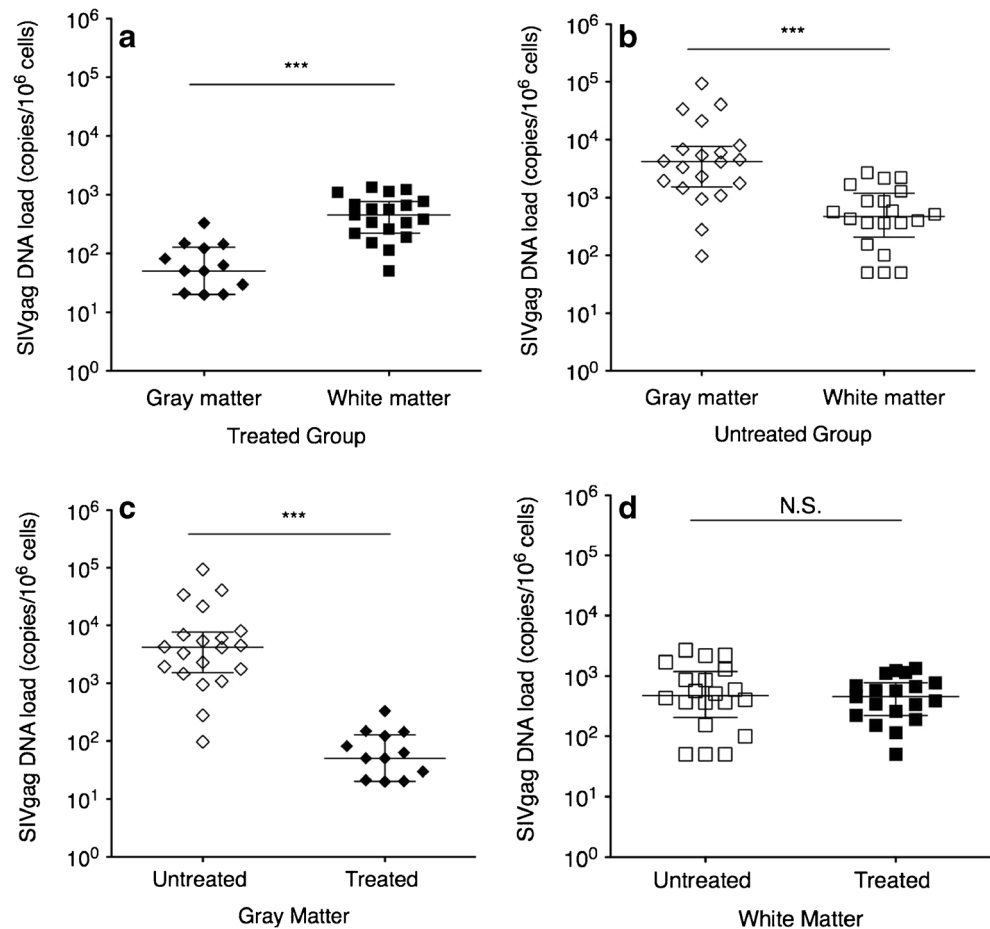
However, strikingly, viral levels were not significantly different between the two groups in white matter, with median 567 copies/10^6 cells in untreated animals versus 530 copies/10^6 cells in treated animals ($p = 0.3494$) (Fig. 2d).

Viral diversity and presence of extensive G-to-A hypermutations in brains of cART animals Next, we assessed the degree of viral mutation and diversity in TPs and cART controllers. We studied two TPs and two of the three DTs (DT1 and DT2). Since the third animal (DT3) in DTs group had very low DNA levels (range of 10 to 10^3 copies/10^6 cells) that were barely measurable by SIV *gag* real-time PCR, PCR quantification of the long fragment of SIV envelope gp120 and sequencing was not obtained from this animal. The limitation of SIV *env* detection is similar to those of single genome analysis (SGA), which can only reliably be successful on plasma samples with viral loads above certain thresholds (~ 4000 copies/ml). Therefore, only those samples that had SIV DNA levels above 1×10^3 copies/10^6 cells in the two TPs and two DTs were analyzed. Overall, the sequences could be easily distinguished between individual animals. Each animal had its own clades of virus (Fig. 3). The sequences from different regions of the brain in TP1 were highly homogeneous and close to the parental strain SIVmac251-PM series

KC522165-KC522168 sequences (Del Prete et al. 2013) shown in Fig. 3. The viral sequences from TP2 were a little more variable and close to KC522142, and the HM045 series (Yeh et al. 2010) with a significant 21 nucleotide deletion in the V4 region in most variants.

Sequences from cART animals DT1 and DT2 clustered closely, and were close to the SIVmac251 sequences of HQ187 series (Whitney et al. 2011) and the parental strain KC522142. Notably, DT2 had a high frequency of APOBEC3G (apolipoprotein B mRNA-editing, enzyme-catalytic, polypeptide-like 3G) hypermutations (G-to-A mutations), up to 75 (p value = 1.40E-11) in sequences derived from two regions: white matter of left parietal lobe and the brain stem (labeled as DT2-22L-W and DT2-24), when compared with sequences from other regions of the same animal and sequences from animal DT1 (Table 4).

Changes of the envelope gp120 of SIV in the CNS in untreated typical progressors and animals on cART To determine if the mutations of nucleotides resulted in amino acid changes in envelope gp120 protein, we further analyzed the amino acid alignment. The sites with most changes were in the V1 and V4 loops. The V1 region was rich in serine (Ser or S) and threonine (Thr or T) especially in cART animals but these
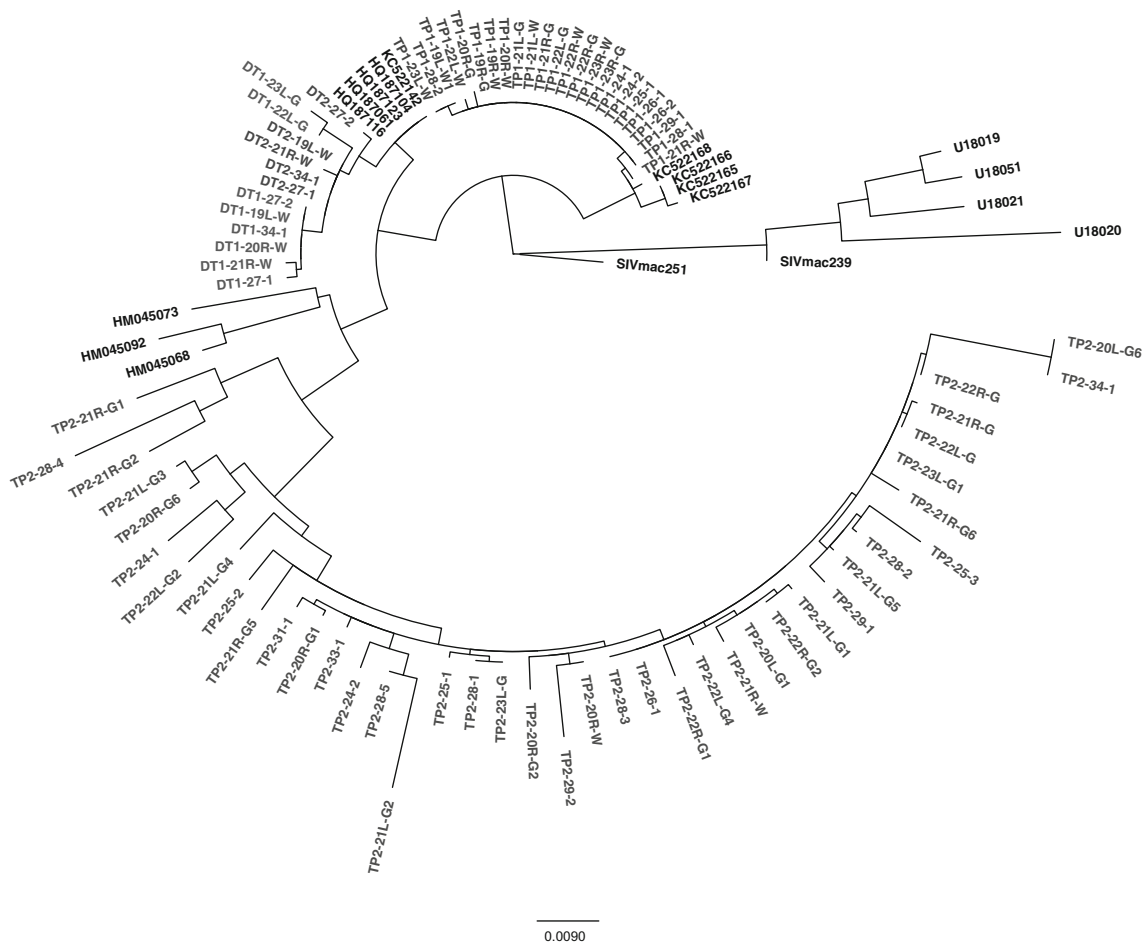
Fig. 3 Phylogenetic analysis of SIV envelope gp120 sequences of variants isolated from gray and white matter of different regions of the brain in 2 SIV-infected typical progressors without cART (TP1 and TP2) and 2 SIV-infected ChRM on cART (DT1 and DT2). Each sequence was named as animal name-label number of the brain followed with the left (L) or right (R) gray or white with more than one sequence if followed with a number, for instance, TP2-20L-G1 (the 2nd typical progressor animal-left temporal lobe-gray matter sequence 1) represents sequence 1 that was isolated from the gray matter of left temporal lobe in the 2nd typical progressor animal. The tree scale bar indicates the number of substitutions per site

were not very glycosylated, which differs from HIV-1M group that have more changes in glycosylation.

Sequences from different regions of the brain of TP2 showed some variations in the V1 and V4 regions. All but one of the TP2 variants had mutations from serine (Ser or S) to proline (Pro or P) at the V1-Loop position 155 (Fig. 4). Further, the V4 loop had a seven amino acid residue deletion at position 424-430 (QRPKERH) corresponding to a 21 nucleotide deletion in the majority of variants (Fig. 4), similar to findings previously reported in virus found in peripheral blood in chronic but not acute phase of SIVmac251 infection (Yeh et al. 2010).

Discussion

To our knowledge, this is the first study to evaluate viral reservoirs in up to 20 variant regions of the CNS in cART-treated

SIV-infected ChRM model of HIV infection, although the SIV/ChRM model has been used to study SIV pathogenesis, as well as tissue reservoirs in lymphoid tissues and the gut (Ling et al. 2010; Ling et al. 2014; Ling et al. 2013; Ling et al. 2007; Ling et al. 2002a; Ling et al. 2002b; Marthas et al. 2001; Monceaux et al. 2007). As ChRM usually have lower viral loads and develop AIDS relatively slower than other SIV-susceptible nonhuman primates, it is not surprising that cVL were not detectable in SIV-infected LTNP of ChRM even prior to cART. However, undetectable cVL clearly did not mean that the virus did not enter the CNS of SIV-infected ChRM, as evidenced by the fact that SIV DNA could be detected in some of the LTNP even after cART. Similar to HIV-1-infected patients, cVL was positively correlated with pVL in typical progressors of ChRM without ART, indicating that ChRM with SIV infection mimics HIV-1 infection in the CNS.

In this study, we found that two sites, basal ganglia and brain stem, had the relatively highest frequencies of SIV

Table 4 Significant hypermutation of G to A in parietal lobe and brain stem in DT2

Sequence	Muts: (match sites)[a]	Controls: (control muts)[b]	Rate ratio[c]	Fisher exact *p* value
DT1-19L-W	8	9	0.89	0.6902
DT1-20R-W	7	9	0.78	0.7786
DT1-21R-W	7	9	0.78	0.7786
DT1-22L-G	4	10	0.4	0.9739
DT1-23L-G	7	10	0.7	0.8404
DT1-27-1	8	9	0.89	0.6902
DT1-34-1	7	9	0.78	0.7786
DT2-19L-W	5	9	0.56	0.9150
DT2-2R-W	4	9	0.44	0.9571
DT2-22L-W	*75*	*21*	*3.62*	*1.40E-11*
DT2-24-1	*75*	*21*	*3.62*	*1.40E-11*
DT2-27-1	4	9	0.44	0.9571
DT2-34-1	4	9	0.44	0.9571

[a] Mutations that match the pattern used in each run. The default pattern is to look for G followed by RD (R = purine = G or A; D = A, G, or T) which is the pattern most often mutated by APOBEC3G

[b] Other mutations that are not in APOBEC sites

[c] The ratio of muts/controls (column 1/column 2)

detection in animals on ART from the 15 parts of the brain and spinal cord tested, indicating that these two sites might be major sites of viral persistence. However, it is possible that some of the viral DNA detected were from defective viruses. Our results are consistent with findings that despite the use of cART, cells carrying viral SIV DNA persist (Zink et al. 2010). In HIV-1-infected patients, abnormalities of the basal ganglia are associated with HIV dementia (Steinbrink et al. 2013). Although detection of viral DNA could not exclude defective virus, the results are still important because even isolated viral particles such as Tat can cause neurocognitive dysfunction, even in the absence of replication-competent virus. Determining which treated animals or treated patients still have substantial CNS reservoir would be very important, as identification and characterization of cellular CNS reservoirs is a critical step to understand the mechanism of viral persistence in the CNS for the development of eradication strategies.

We found significant differences in SIV DNA viral loads between gray and white matter in the same group of animals in untreated as well as cART animals as shown in Fig. 2. We also found that no significant differences in white matter viral loads between untreated and cART animals (Fig. 2d). Since the animals were not perfused when euthanized, it is possible that viruses examined in the gray matter could also contain vessel-associated blood-derived virus, as the human brain has higher blood flow in the gray matter than that of the white matter (Ballabh et al. 2004; Rengachary and Ellenbogen 2005). However, the > 2-fold log10 disparity of SIV load between untreated and treated was unlikely due solely to virus from blood contamination. The results

suggested that antiretroviral therapy was effective in reducing viral DNA loads in the gray matter.

In contrast, the comparable viral levels in white matter between cART macaques and untreated group indicate that cART has little impact on this tissue, possibly due to poor penetration of antiretroviral drugs (Cory et al. 2013; Letendre et al. 2008). This result is in agreement with observations that HIV is more compartmentalized in the subcortical white matter in HIV-infected patients on cART (Nath 2015). A number of studies have demonstrated that gray matter and/or white matter undergo significant structural alterations during HIV infection, even in patients receiving cART (Becker et al. 2012; Fennema-Notestine et al. 2013; Sarma et al. 2014; Wang et al. 2016). Although cellular reservoirs in the CNS are not fully understood, studies have suggested that cellular HIV or SIV reservoirs in the CNS likely include perivascular macrophages, long-lived microglia cells (Dahl et al. 2014; Schnell et al. 2009; Williams et al. 2001) and astrocytes (Churchill et al. 2009). Further, there are more microglia in white matter than gray matter in the human brain (Mittelbronn et al. 2001). Based on the brain regions we studied, the microglial populations harboring SIV in these two regions are the most likely major factors contributing to the differences in virus loads observed between gray and white matter.

While viral diversity and CNS compartmentalization (in CSF) have been identified in multiple studies (Sturdevant et al. 2012; Sturdevant et al. 2015), especially in HIV-1-infected patients with HIV-associated dementia (HAD) (Schnell et al. 2011) and during the early years after HIV transmission (Schnell et al. 2010), here we mainly focused on viral variants isolated from different specific regions of
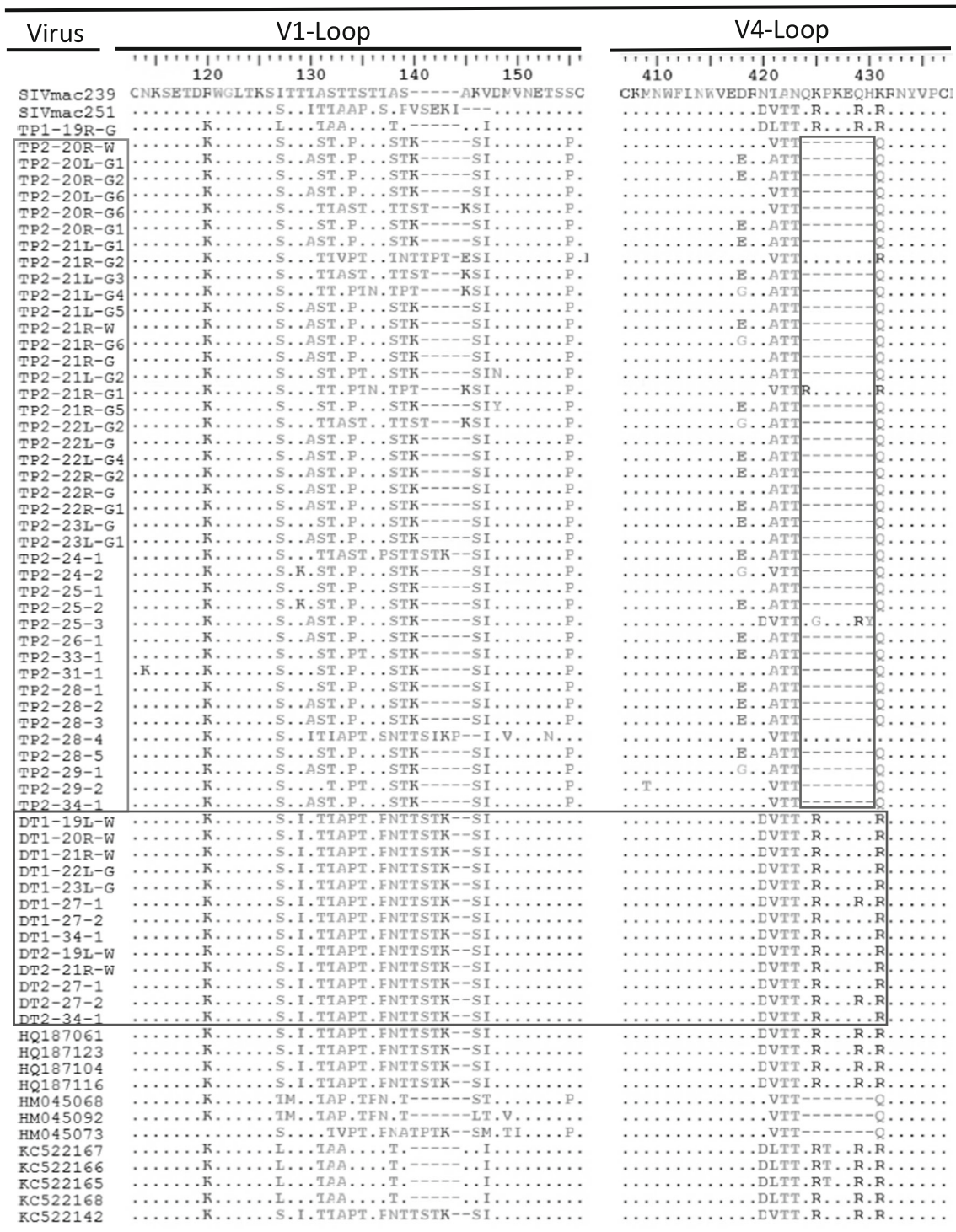
Fig. 4 Amino acid sequence comparison of SIV envelope V1 loop and V4 loop of SIVmac239, SIVmac251, variants from each sample group. TP1, test animal 1 (representative sequence); TP2, test animal 2; DT1, drug-treated animal 1; DT2, drug-treated animal 2. HQ series and HM series, GenBank sequences; and KC strains, parental strains. Dots represent amino acid identity with reference strain SIVmac239; dashes represent deletions

the brain. We found that each animal had its own clade of viruses, which agrees with the vast majority of other HIV and SIV data sets that suggest even if a person or animal is exposed to viral quasi-species from a donor, or from an experimental stock of SIV, primary infections in the recipient are almost always essentially clonal. TP1 appears to have a bottleneck effect that indicates a homogenous population was formed in the brain tissues both in white and gray matter. This

is probably due to the brain blood barrier (BBB) selection effect, and that particular virus may have had the best fit in these brain tissues. Although TP2 showed relatively more diversification, dominant variants had a specific 21 nucleotide deletion in V4 region which was not found in parental virus stock, similar to findings from chronically SIVmac251-infected macaques, which the HM045 series sequences reported elsewhere (Yeh et al. 2010) and a 15 nucleotide deletion at the same region in sequences of U18019-U18021 series (Zhu et al. 1995), suggesting the mutated virus is likely emerging in chronic infection. Whether the mutation occurred after virus entered the brain or was derived from peripheral blood in chronic infection or whether the mutated virus is the source of blood mutated virus remains to be determined, especially since other studies have demonstrated that meninges contain both CNS and peripheral blood-derived viruses (Matsuda et al. 2013), and there is a possibility of viral dissemination from the brain to the blood, or from the meninges to the brain parenchyma (Nath 2015). Since the function of V4 loop is not well understood, it is unclear whether there is selective pressure on the variants to shorten the V4 loop by 7 residues (QRPKERH). However, further studies are needed to elucidate the virological and immunological significance of this shortening of the V4 loop.

Interestingly, sequences from white matter of the left parietal lobe and brain stem (22L-W and 24-W) in animal DT2 had high frequencies of G to A mutations (calculate p value, Table 2). These findings are in agreement with results in viral sequences isolated from brain (Depboylu et al. 2007) and semen of SIV-infected rhesus macaques (Whitney et al. 2011) as well as in HIV-1-infected patients receiving antiretroviral drugs (Knoepfel et al. 2011; Mullins et al. 2011), possibly because of APOBEC3G editing under the selective pressure of drug treatment. While most of these viruses could be defective, DNA genome-like G-to-A mutated viruses have been detected in blood and rectal tissue (Fourati et al. 2012), and it is noteworthy that the G-to-A mutations were found only in the parietal lobe and brain stem, but no other sections of the brain in this animal, suggesting that viral hypermutation does not simultaneously occur in different sections of the brain.

Here, we show that SIV-infected ChRM on cART are an excellent model to study neuro-AIDS and CNS reservoirs. Moreover, given that the virus enters the CNS as early as days after infection (Valcour et al. 2012), and pVL are comparable during acute infection between Indian rhesus macaques and ChRM even those become spontaneous LTNP (Ling et al. 2002a), we show that the CNS reservoir is established and persistent after SIV infection in both progressors and LTNP of ChRM. Of note, not all animals have detectable virus in the CNS, just like HIV-1-infected patients, many of whom also do not have detectable virus in brain tissues (Zhao et al. 2009).

We also show that basal ganglia and brain stem may be the major sites of viral persistence in the CNS after antiretroviral therapy. Moreover, cART group had significantly reduced viral levels in gray matter but had no significant changes in viral levels in white matter when compared with untreated macaques. Finally, G to A hypermutations occurred in certain parts of the brain in a cART animal. Therefore, sampling multiple regions of the CNS may be necessary when assessing effects of novel approaches on reduction of the size of viral reservoirs in the CNS. Of note, we only used PMPA and FTC in this study, effect of more potent regimen of cART on CNS reservoir, such as the clinically recommended combination of tenofovir disoproxil fumarate (TDF)/emtricitabine (FTC)/dolutegravir (DTG), can be thoroughly tested in this unique nonhuman primate model of HIV infection.

Materials and methods

Ethics statement Experimental procedures performed on rhesus macaques used in this study were approved by the Tulane Institutional Animal Care and Use Committee (IACUC). All animals were housed indoors throughout the study period at the Tulane National Primate Research Center (TNPRC). TNPRC facilities are fully accredited by the Association of Assessment and Accreditation of Laboratory Animal Care International (AAALAC) in accordance with standard husbandry practices following the Guide for the Care and Use of Laboratory Animals (NIH). To avoid unnecessary discomfort and pain to animals, anesthesia and analgesic medications were used appropriately under the direction of a veterinarian. Rhesus macaques were anesthetized with 10 mg/kg ketamine or 3–8 mg/kg telazol whenever they were removed from their home cage. For surgical procedures, animals were anesthetized with ketamine and maintained in a surgical plane of anesthesia using isoflurane. For physical exams and blood sampling, 10 mg/kg ketamine was used. Buprenorphine (0.01 mg/kg) or buprenorphine extended release (0.2 mg/kg) was the standard analgesics administered for painful procedures.

Animals and virus inoculation Rhesus macaques (*Macaca mulatta*) of Chinese origin (ChRM) were used in this study. A total of 23 animals were studied, which included 11 out of 12 SIV-infected DTs with exclusion of the one that had detectable viral load at necropsy, and also included 12 chronically SIV-infected untreated animals for CSF and blood collection to monitor viral loads in plasma and cerebrospinal fluid (CSF). The 11 DTs were further studied from 15 brain regions described in details below in brain tissue collection. Two representative untreated animals were also studied from 15 brain regions for comparison. These two animals were typical progressors (TPs), which were infected for 1–3 years with a

set point plasma viral loads at $10^4 \sim 10^6$ copies/ml. Basic animal information is shown in Table 1 for treated animals and Table 2 for untreated animals. Animals were intravaginally or intravenously infected with 500 TCID$_{50}$ SIVmac251. The stock SIVmac251 was obtained by culturing and harvesting from CEMx174 cells and provided by the Virus Characterization, Isolation, and Production Core of the TNPRC, and the sequences of the stock are available in GenBank (KC522165-168, KC522142) (Del Prete et al. 2013).

Antiretroviral therapy During chronic SIV infection, 11 ChRM were treated with the reverse transcriptase inhibitors (R)-9-(2-phosphonylmethoxyypropyl) adenine (PMPA, tenofovir; 20 mg/kg), and beta-2′, 3′ dideoxy-3′-thia-5-fluorocytidine (FTC, emtricitabine; 40 mg/kg) daily by subcutaneous injection for 8–24 weeks. Tenofovir and emtricitabine were generously provided by Gilead Sciences, Inc. (Foster City, CA) via Material Transfer Agreement.

Animal euthanasia and brain tissue collection Animal euthanasia was consistent with the recommendations of the Panel on Euthanasia of the American Veterinary Medical Association. SIV-infected and/or drug-treated macaques were euthanized by first anesthetizing the animal with telazol and buprenorphine followed by a lethal i.v. injection of sodium pentobarbital following Tulane IACUC standards of operation (SOP). Tissues from brain and spinal cord (15 regions) were collected fresh and also snap frozen in liquid nitrogen during necropsies.

Quantification of viral RNA in plasma and cerebrospinal fluid in brain tissues Plasma was separated from EDTA-treated whole blood by centrifugation at 700–800×g for 10 min, conservatively removed plasma to avoid cell pellet, transferred to a second centrifuge tube, and were centrifuged at 25,000×g for 1 h to concentrate virus particles especially in samples from animals on cART with expected low viral loads. CSF was obtained from the dorsal cervical spine using TNPRC's standard operating procedures. CSF was centrifuged following the similar procedures as collection of plasma. SIV plasma viral loads (pVL) and CSF viral loads (cVL) were determined by real-time quantitative PCR analysis by the TNPRC Pathogen Detection and Quantification Core as described in detail elsewhere (Monjure et al. 2014). High Pure Viral RNA kit (Roche, Indianapolis, IN, USA) was used for viral RNA extraction with minor modification. Primers and probe were designed from the conserved gag region covering detection of SIVmac239, SIVmac251, and SHIV viruses.

DNA extraction and quantification of viral DNA in brain tissues Total genomic DNA was extracted from each tissue using a QIAamp DNA mini kit following the manufacturer's instructions. Determination of cell-associated SIV DNA viral loads for samples collected up to the time of necropsy followed methods for assays and analysis previously described elsewhere (Venneti et al. 2008). These standard methods have a 95% reliable threshold sensitivity of 30 total copies of SIV DNA or RNA per sample. Numbers of SIV copies were normalized to cell equivalents co-determined by quantitative PCR (qPCR) as described (Ling et al. 2014). For samples prepared from necropsy tissues, nested and qPCR/RT-PCR methods of analysis with reaction conditions and primer/probe sequences were performed as detailed in Hansen et al. (Hansen et al. 2011). DNA was prepared as above from multiple tissues to provide a greater amount of test material and a correspondingly lower limit of detection.

Viral DNA amplification by nested PCR, sequencing, and phylogenetic analysis One to 0.5 μg DNA was used for nested PCR to amplify SIV *envelope* gp120. The PCR products were purified using Clonetech PCR purification kit for population-based sequencing. Expand High Fidelity PCR (Taqman enzyme) was used to minimize PCR-induced sequence errors. The primers were as below:

env-OF: 5′ CTATAATAGACATGGAGACACCCTTG 3′
env-OR: 5′ CTTCTTGCACTGTAATAAATCCCTTCC 3′
env-iF: 5′ GTAAAAAGTGTTGCTACCATTGCCAG 3′
env-iR: 5′ ACTGATACCCCTACCAAGTCATC 3′

PCR reaction conditions included denaturation at 94 °C for 2 min, followed by 35 cycles of denaturation at 94 °C for 50 s, annealing at 55 °C for 50 s, and extension at 72 °C for 2 min, with an additional extension of 72 °C for 7 min. Two microliters of the first-round PCR products was used for nested PCR under the same thermocycling parameters. The PCR products were purified using high pure PCR product purification kit from Roche Life Science. SIV gp120 *env* sequences from newly isolated brain SIV variants were aligned with SIVmac239, and SIVmac251 reference sequences from the Los Alamos National Laboratory HIV Sequence Database and other relevant sequences from GenBank using the CLUSTAL X program (Thompson et al. 1997). The alignment was manually adjusted, and poorly aligned regions were excluded. All phylogenetic trees were constructed by PhyML program for a maximum likelihood tree starting with BioNJ neighbor-joining method, and the reproducibility of the branching orders was estimated by 1000 bootstraps. Frequencies of G-to-A mutations were analyzed using the HIV Sequence Database Hypermut 2.0 program (http://hiv-web.lanl.gov). The amino acid sequences were aligned using Clustal W program of the BioEdit software. Highlighter for amino acid sequences v2.3.4 and analysis (Keele et al. 2008) was used to visualize the differences in amino acids between untreated and treated animals.

Statistical analysis Nonparametric statistical analyses (Mann-Whitney test or Wilcoxon signed-rank test) were used to compare median viral loads in plasma and CSF, cell-associated SIV DNA in gray matter versus white matter, and untreated versus drug-treated groups. The Spearman correlation was used to assess the relationship of levels of viral loads between plasma and CSF. GraphPad Prism 5.0 statistical software (GraphPad Software, Inc. San Diego, CA, USA) was used to analyze data and statistical results were set two-sided at $p < 0.05$ as significant.

Nucleotide sequence accession numbers Viral *env* sequences were deposited in GenBank under accession numbers MF284715-MF284792.

Compliance with ethical standards Experimental procedures performed on rhesus macaques used in this study were approved by the Tulane Institutional Animal Care and Use Committee (IACUC). All animals were housed indoors throughout the study period at the Tulane National Primate Research Center (TNPRC). TNPRC facilities are fully accredited by the Association of Assessment and Accreditation of Laboratory Animal Care International (AAALAC) in accordance with standard husbandry practices following the Guide for the Care and Use of Laboratory Animals (NIH).

Disclaimer The content is solely the responsibility of the authors and does not necessarily represent the official views of the National Institutes of Health.

Conflict of interest The authors declare that they have no conflict of interest.

References

Ballabh P, Braun A, Nedergaard M (2004) Anatomic analysis of blood vessels in germinal matrix, cerebral cortex, and white matter in developing infants. Pediatr Res 56:117–124

Becker JT, Maruca V, Kingsley LA, Sanders JM, Alger JR, Barker PB, Goodkin K, Martin E, Miller EN, Ragin A, Sacktor N, Selnes O, Multicenter ACS (2012) Factors affecting brain structure in men with HIV disease in the post-HAART era. Neuroradiology 54:113–121

Brew BJ, Robertson K, Wright EJ, Churchill M, Crowe SM, Cysique LA, Deeks S, Garcia JV, Gelman B, Gray LR, Johnson T, Joseph J, Margolis DM, Mankowski JL, Spencer B (2015) HIV eradication symposium: will the brain be left behind? J Neuro-Oncol 21:322–334

Churchill M, Nath A (2013) Where does HIV hide? A focus on the central nervous system. Curr Opin HIV AIDS 8:165–169

Churchill MJ, Deeks SG, Margolis DM, Siliciano RF, Swanstrom R (2016) HIV reservoirs: what, where and how to target them. Nat Rev Microbiol 14:55–60

Churchill MJ, Wesselingh SL, Cowley D, Pardo CA, McArthur JC, Brew BJ, Gorry PR (2009) Extensive astrocyte infection is prominent in human immunodeficiency virus-associated dementia. Ann Neurol 66:253–258

Clements JE, Gama L, Graham DR, Mankowski JL, Zink MC (2011) A simian immunodeficiency virus macaque model of highly active antiretroviral treatment: viral latency in the periphery and the central nervous system. Curr Opin HIV AIDS 6:37–42

Cory TJ, Schacker TW, Stevenson M, Fletcher CV (2013) Overcoming pharmacologic sanctuaries. Curr Opin HIV AIDS 8:190–195

Dahl V, Gisslen M, Hagberg L, Peterson J, Shao W, Spudich S, Price RW, Palmer S (2014) An example of genetically distinct HIV type 1 variants in cerebrospinal fluid and plasma during suppressive therapy. J Infect Dis 209:1618–1622

Del Prete GQ, Scarlotta M, Newman L, Reid C, Parodi LM, Roser JD, Oswald K, Marx PA, Miller CJ, Desrosiers RC, Barouch DH, Pal R, Piatak M Jr, Chertova E, Giavedoni LD, O'Connor DH, Lifson JD, Keele BF (2013) Comparative characterization of transfection- and infection-derived simian immunodeficiency virus challenge stocks for in vivo nonhuman primate studies. J Virol 87:4584–4595

Depboylu C, Eiden LE, Weihe E (2007) Increased APOBEC3G expression is associated with extensive G-to-A hypermutation in viral DNA in rhesus macaque brain during lentiviral infection. J Neuropathol Exp Neurol 66:901–912

Eden A, Fuchs D, Hagberg L, Nilsson S, Spudich S, Svennerholm B, Price RW, Gisslen M (2010) HIV-1 viral escape in cerebrospinal fluid of subjects on suppressive antiretroviral treatment. J Infect Dis 202:1819–1825

Fennema-Notestine C, Ellis RJ, Archibald SL, Jernigan TL, Letendre SL, Notestine RJ, Taylor MJ, Theilmann RJ, Julaton MD, Croteau DJ, Wolfson T, Heaton RK, Gamst AC, Franklin DR Jr, Clifford DB, Collier AC, Gelman BB, Marra C, McArthur JC, McCutchan JA, Morgello S, Simpson DM, Grant I, Group C (2013) Increases in brain white matter abnormalities and subcortical gray matter are linked to CD4 recovery in HIV infection. J Neuro-Oncol 19:393–401

Fourati S, Lambert-Niclot S, Soulie C, Malet I, Valantin MA, Descours B, Ait-Arkoub Z, Mory B, Carcelain G, Katlama C, Calvez V, Marcelin AG (2012) HIV-1 genome is often defective in PBMCs and rectal tissues after long-term HAART as a result of APOBEC3 editing and correlates with the size of reservoirs. J Antimicrob Chemother 67:2323–2326

Garrido C, Margolis DM (2015) Translational challenges in targeting latent HIV infection and the CNS reservoir problem. J Neuro-Oncol 21:222–226

Hansen SG, Ford JC, Lewis MS, Ventura AB, Hughes CM, Coyne-Johnson L, Whizin N, Oswald K, Shoemaker R, Swanson T, Legasse AW, Chiuchiolo MJ, Parks CL, Axthelm MK, Nelson JA, Jarvis MA, Piatak M Jr, Lifson JD, Picker LJ (2011) Profound early control of highly pathogenic SIV by an effector memory T-cell vaccine. Nature 473:523–527

Heaton RK, Clifford DB, Franklin DR Jr, Woods SP, Ake C, Vaida F, Ellis RJ, Letendre SL, Marcotte TD, Atkinson JH, Rivera-Mindt M, Vigil OR, Taylor MJ, Collier AC, Marra CM, Gelman BB, McArthur JC, Morgello S, Simpson DM, McCutchan JA, Abramson I, Gamst A, Fennema-Notestine C, Jernigan TL, Wong J, Grant I (2010) HIV-associated neurocognitive disorders persist in the era of potent antiretroviral therapy: CHARTER Study. Neurology 75:2087–2096

Keele BF, Giorgi EE, Salazar-Gonzalez JF, Decker JM, Pham KT, Salazar MG, Sun C, Grayson T, Wang S, Li H, Wei X, Jiang C, Kirchherr JL, Gao F, Anderson JA, Ping LH, Swanstrom R, Tomaras GD, Blattner WA, Goepfert PA, Kilby JM, Saag MS, Delwart EL,

Busch MP, Cohen MS, Montefiori DC, Haynes BF, Gaschen B, Athreya GS, Lee HY, Wood N, Seoighe C, Perelson AS, Bhattacharya T, Korber BT, Hahn BH, Shaw GM (2008) Identification and characterization of transmitted and early founder virus envelopes in primary HIV-1 infection. Proc Natl Acad Sci U S A 105:7552–7557

Knoepfel SA, Di Giallonardo F, Daumer M, Thielen A, Metzner KJ (2011) In-depth analysis of G-to-A hypermutation rate in HIV-1 env DNA induced by endogenous APOBEC3 proteins using massively parallel sequencing. J Virol Methods 171:329–338

Letendre S, Marquie-Beck J, Capparelli E, Best B, Clifford D, Collier AC, Gelman BB, JC MA, McCutchan JA, Morgello S, Simpson D, Grant I, Ellis RJ, Group C (2008) Validation of the CNS penetration-effectiveness rank for quantifying antiretroviral penetration into the central nervous system. Arch Neurol 65:65–70

Ling B, Mohan M, Lackner AA, Green LC, Marx PA, Doyle LA, Veazey RS (2010) The large intestine as a major reservoir for simian immunodeficiency virus in macaques with long-term, nonprogressing infection. J Infect Dis 202:1846–1854

Ling B, Piatak M Jr, Rogers L, Johnson A-M, Russell-Lodrigue K, Hazuda DJ, Lifson JD, Veazey RS (2014) Effects of treatment with suppressive combination antiretroviral drug therapy and the histone deacetylase inhibitor suberoylanilide hydroxamic acid; (SAHA) on SIV-infected Chinese rhesus macaques. PLoS One 9:e102795

Ling B, Rogers L, Johnson AM, Piatak M, Lifson J, Veazey RS (2013) Effect of combination antiretroviral therapy on Chinese rhesus macaques of simian immunodeficiency virus infection. AIDS Res Hum Retrovir 29:1465–1474

Ling B, Veazey RS, Hart M, Lackner AA, Kuroda M, Pahar B, Marx PA (2007) Early restoration of mucosal CD4 memory CCR5 T cells in the gut of SIV-infected rhesus predicts long term non-progression. AIDS 21:2377–2385

Ling B, Veazey RS, Luckay A, Penedo C, Xu K, Lifson JD, Marx PA (2002a) SIV(mac) pathogenesis in rhesus macaques of Chinese and Indian origin compared with primary HIV infections in humans. AIDS 16:1489–1496

Ling B, Veazey RS, Penedo C, Xu K, Lifson JD, Marx PA (2002b) Longitudinal follow up of SIVmac pathogenesis in rhesus macaques of Chinese origin: emergence of B cell lymphoma. J Med Primatol 31:154–163

Liu H, Xiao QH, Liu JB, Li JL, Zhou L, Xian QY, Wang Y, Zhang J, Wang X, Ho WZ, Zhuang K (2016) SIV infection impairs the central nervous system in Chinese rhesus macaques. J NeuroImmune Pharmacol 11:592–600

Marthas ML, Lu D, Penedo MC, Hendrickx AG, Miller CJ (2001) Titration of an SIVmac251 stock by vaginal inoculation of Indian and Chinese origin rhesus macaques: transmission efficiency, viral loads, and antibody responses. AIDS Res Hum Retrovir 17:1455–1466

Matsuda K, Brown CR, Foley B, Goeken R, Whitted S, Dang Q, Wu F, Plishka R, Buckler-White A, Hirsch VM (2013) Laser capture microdissection assessment of virus compartmentalization in the central nervous systems of macaques infected with neurovirulent simian immunodeficiency virus. J Virol 87:8896–8908

Mittelbronn M, Dietz K, Schluesener HJ, Meyermann R (2001) Local distribution of microglia in the normal adult human central nervous system differs by up to one order of magnitude. Acta Neuropathol 101:249–255

Monceaux V, Viollet L, Petit F, Cumont MC, Kaufmann GR, Aubertin AM, Hurtrel B, Silvestri G, Estaquier J (2007) CD4+ CCR5+ T-cell dynamics during simian immunodeficiency virus infection of Chinese rhesus macaques. J Virol 81:13865–13875

Monjure CJ, Tatum CD, Panganiban AT, Arainga M, Traina-Dorge V, Marx PA Jr, Didier ES (2014) Optimization of PCR for quantification of simian immunodeficiency virus genomic RNA in plasma of rhesus macaques (Macaca mulatta) using armored RNA. J Med Primatol 43:31–43

Mullins JI, Heath L, Hughes JP, Kicha J, Styrchak S, Wong KG, Rao U, Hansen A, Harris KS, Laurent JP, Li D, Simpson JH, Essigmann JM, Loeb LA, Parkins J (2011) Mutation of HIV-1 genomes in a clinical population treated with the mutagenic nucleoside KP1461. PLoS One 6:e15135

Nath A (2015) Eradication of human immunodeficiency virus from brain reservoirs. J Neuro-Oncol 21:227–234

Rengachary SS, Ellenbogen RG (2005) Principles of neurosurgery, 2nd edn. Elsevier Mosby, Edinburgh; New York

Sarma MK, Nagarajan R, Keller MA, Kumar R, Nielsen-Saines K, Michalik DE, Deville J, Church JA, Thomas MA (2014) Regional brain gray and white matter changes in perinatally HIV-infected adolescents. Neuroimage Clin 4:29–34

Schnell G, Joseph S, Spudich S, Price RW, Swanstrom R (2011) HIV-1 replication in the central nervous system occurs in two distinct cell types. PLoS Pathog 7:e1002286

Schnell G, Price RW, Swanstrom R, Spudich S (2010) Compartmentalization and clonal amplification of HIV-1 variants in the cerebrospinal fluid during primary infection. J Virol 84:2395–2407

Schnell G, Spudich S, Harrington P, Price RW, Swanstrom R (2009) Compartmentalized human immunodeficiency virus type 1 originates from long-lived cells in some subjects with HIV-1-associated dementia. PLoS Pathog 5:e1000395

Steinbrink F, Evers S, Buerke B, Young P, Arendt G, Koutsilieri E, Reichelt D, Lohmann H, Husstedt IW, German Competence Network HA (2013) Cognitive impairment in HIV infection is associated with MRI and CSF pattern of neurodegeneration. Eur J Neurol 20:420–428

Sturdevant CB, Dow A, Jabara CB, Joseph SB, Schnell G, Takamune N, Mallewa M, Heyderman RS, Van Rie A, Swanstrom R (2012) Central nervous system compartmentalization of HIV-1 subtype C variants early and late in infection in young children. PLoS Pathog 8:e1003094

Sturdevant CB, Joseph SB, Schnell G, Price RW, Swanstrom R, Spudich S (2015) Compartmentalized replication of R5 T cell-tropic HIV-1 in the central nervous system early in the course of infection. PLoS Pathog 11:e1004720

Thompson JD, Gibson TJ, Plewniak F, Jeanmougin F, Higgins DG (1997) The CLUSTAL_X windows interface: flexible strategies for multiple sequence alignment aided by quality analysis tools. Nucleic Acids Res 25:4876–4882

Valcour V, Chalermchai T, Sailasuta N, Marovich M, Lerdlum S, Suttichom D, Suwanwela NC, Jagodzinski L, Michael N, Spudich S, van Griensven F, de Souza M, Kim J, Ananworanich J, Group RSS (2012) Central nervous system viral invasion and inflammation during acute HIV infection. J Infect Dis 206:275–282

Venneti S, Bonneh-Barkay D, Lopresti BJ, Bissel SJ, Wang G, Mathis CA, Piatak M Jr, Lifson JD, Nyaundi JO, Murphey-Corb M, Wiley CA (2008) Longitudinal in vivo positron emission tomography imaging of infected and activated brain macrophages in a macaque model of human immunodeficiency virus encephalitis correlates with central and peripheral markers of encephalitis and areas of synaptic degeneration. Am J Pathol 172:1603–1616

Wang B, Liu Z, Liu J, Tang Z, Li H, Tian J (2016) Gray and white matter alterations in early HIV-infected patients: combined voxel-based morphometry and tract-based spatial statistics. J Magn Reson Imaging 43:1474–1483

Whitney JB, Hraber PT, Luedemann C, Giorgi EE, Daniels MG, Bhattacharya T, Rao SS, Mascola JR, Nabel GJ, Korber BT, Letvin NL (2011) Genital tract sequestration of SIV following acute infection. PLoS Pathog 7:e1001293

Williams KC, Corey S, Westmoreland SV, Pauley D, Knight H, deBakker C, Alvarez X, Lackner AA (2001) Perivascular macrophages are the

primary cell type productively infected by simian immunodeficiency virus in the brains of macaques: implications for the neuropathogenesis of AIDS. J Exp Med 193:905–915

Yeh WW, Rahman I, Hraber P, Coffey RT, Nevidomskyte D, Giri A, Asmal M, Miljkovic S, Daniels M, Whitney JB, Keele BF, Hahn BH, Korber BT, Shaw GM, Seaman MS, Letvin NL (2010) Autologous neutralizing antibodies to the transmitted/founder viruses emerge late after simian immunodeficiency virus SIVmac251 infection of rhesus monkeys. J Virol 84:6018–6032

Zhao L, Galligan DC, Lamers SL, Yu S, Shagrun L, Salemi M, McGrath MS (2009) High level HIV-1 DNA concentrations in brain tissues differentiate patients with post-HAART AIDS dementia complex or cardiovascular disease from those with AIDS. Sci China C Life Sci 52:651–656

Zhou Y, Bao R, Haigwood NL, Persidsky Y, Ho WZ (2013) SIV infection of rhesus macaques of Chinese origin: a suitable model for HIV infection in humans. Retrovirology 10:89

Zhu GW, Liu ZQ, Joag SV, Pinson DM, Adany I, Narayan O, McClure HM, Stephens EB (1995) Pathogenesis of lymphocyte-tropic and macrophage-tropic SIVmac infection in the brain. J Neuro-Oncol 1:78–91

Zink MC, Brice AK, Kelly KM, Queen SE, Gama L, Li M, Adams RJ, Bartizal C, Varrone J, Rabi SA, Graham DR, Tarwater PM, Mankowski JL, Clements JE (2010) Simian immunodeficiency virus-infected macaques treated with highly active antiretroviral therapy have reduced central nervous system viral replication and inflammation but persistence of viral DNA. J Infect Dis 202:161–170